IIETA International Information and Engineering Technology Association
Advancing the World of Information and Engineering

Revue des Composites et des Matériaux Avancés-Journal of Composite and Advanced Materials
Vol. 35, No. 1, February, 2025, pp. 143-154
Journal homepage: http://iieta.org/journals/rcma

Fatigue Behavior under Constant Load of CFRP Sheets Compared to Their Performance under Static Load

Fadhil Talib. Salman*, Enaam Obeid. Hassoun, Majida Khaleel. Ahmed

Electromechanical Engineering Department, University of Technology, Baghdad 10066, Iraq

Corresponding Author Email: eme.22.34@grad.uotechnology.edu.iq

Copyright: ©2025 The authors. This article is published by IIETA and is licensed under the CC BY 4.0 license (http://creativecommons.org/licenses/by/4.0/).

https://doi.org/10.18280/rcma.350117

Received: 14 January 2025
Revised: 10 February 2025
Accepted: 20 February 2025
Available online: 28 February 2025

Keywords:
CFRP, accumulation of damage, static loading, LCF

ABSTRACT

Carbon fiber reinforced polymer (CFRP) composites are widely used in engineering applications due to their exceptional strength-to-weight ratio. These composites are subjected to various loads, both constant and variable, which makes them susceptible to damage accumulation in their structure. This reduces their service life and negatively affects their performance. This study investigates the failure behavior of CFRP laminates under constant loads for one specimen and variable loads using the low-cycle fatigue (LCF) procedure for another until complete failure is achieved in both tests. The experimental procedure involved the use of a specially designed apparatus to apply loads through internal air pressure to the center of the panel once it is securely fixed in place. The observed deformation of the specimen was tracked in line with its maximum deflection measurements. The experimental results showed good agreement with the theoretical results. The maximum deflection of the specimen under static loading at the moment of failure of the specimen was (8.975 mm); in comparison, the maximum deflection of the specimen under low-cycle fatigue at the moment of failure of the specimen was (12.32 mm) after the internal structure of the specimen gradually deteriorated before the complete collapse of the specimen. The specimen was analyzed using a scanning electron microscope (SEM) after failure under a low-cycle fatigue (LCF) test. Hardness tests were conducted before and after the experimental work to track the failure mechanisms, which included gradual failure stages. The results and discussion will detail a noticeable deterioration in the hardness of the material. The experimental results showed good agreement with theoretical values and advanced insights into understanding the failure mechanisms and safety limits in both tests of the composite material.

1. INTRODUCTION

The theoretical strength of materials is often greater than their actual strength; homogeneous metals and their alloys may not always meet the needs of modern and advanced technologies; only a combination of several materials Will meet the performance criteria. Therefore, composites feature thin-diameter, high-performance reinforcements inserted into a matrix material, such as epoxy [1]. In composites, materials are systematically combined to improve their strengths and mitigate the effects of their weaknesses. The optimisation process allows designers to move beyond the limitations tied to the selection and production of traditional materials [2]. Fiber-reinforced polymers are being adopted more frequently in multiple engineering fields, such as aerospace, transportation, sports, and the manufacturing of body armor and helmets. Thus, understanding their impact behavior is crucial for assessing their reliability [3]. The aim of creating composites is to develop a lightweight material that exhibits enhanced mechanical properties, which cannot be achieved by the individual components alone. The interactions in the inter-phase region between the matrix and reinforcing materials, along with the material's microstructure, are the key factors influencing the enhanced properties of the composite [4]. Recent studies have examined the effects of different loading modes on composite structures, including impact, internal and external pressure, and static and quasi-static loads [5]. When a structural element is unable to perform the function for which it was designed while still complying with the required safety margins, it is said to have failed. Fracture of the material is an obvious example of failure; nevertheless, it is not the only sort of failure that may occur. Fracture of composite materials is difficult because of their microscopic structure and anisotropic properties, which make the process of fracture more complicated [6]. CFRP's mechanical properties may be impaired by different environmental conditions encountered in certain applications. In addition, it is exposed to different loads or increased stresses [7]. Polymer matrix composites exhibit a tendency to experience increasing deformation when subjected to constant loads [8]. Likewise, when a material is subjected to cyclic stress, it undergoes fatigue, which progressively weakens it and may eventually lead to fractures

and damage. Although composites are designed to be unaffected by fatigue, they are still susceptible to fatigue loads. The importance of understanding and predicting the fatigue life of composites is due, in part, to the fact that composite failure occurs rapidly and without warning [9].

Fatigue refers to the deterioration of a material that takes place when it experiences repeated cyclic loading. Following several loads, the material starts to deteriorate, resulting in the emergence of fractures and various defects [10]. In addition, low-cycle fatigue is markedly different in terms of fatigue damage. Both the high-stress and the low-cycle fatigue in CFRP lead to irreparable damage. In high-cycle fatigue scenarios, the stress levels are sufficiently low to ensure that the material remains within its elastic proportionality limits, resulting in the gradual fatigue damage of composites. The intricate process of material fatigue can be categorised into three specific stages: crack nucleation, micro-crack growth, and macro-macro growth. The accumulation of micro-damage within the material can progressively develop into macro-cracks, ultimately resulting in macro-scale damage that leads to the material's failure [11]. Every design procedure has to account for fatigue and associated phenomena, as they are the leading causes of engineering structure failures [12].

The primary factor contributing to this phenomenon in composites is the buildup of damage; compared to fatigue failure of metals, fatigue failure of composites is more unpredictable [13].

The outcomes observed stem from the interplay of damage modes, such as matrix failure, fiber pull-out, fracture, and delamination. Defects in the material that arise during the manufacturing process represent another contributing factor to fatigue. Defects include wrinkles, misalignment of fibers, and voids [12].

These defects have the potential to work as sites for fatigue failure [14].

The characteristics suddenly decrease to an acceptable value in line with the failure criterion, rendering the failing section incapable of supporting the load. The cyclic loading of composites leads to a consistent decline in their stiffness and strength, forming the foundation of the gradual deterioration rule [15]. The laminate's thickness influences its sensitivity to fatigue, which accumulates over time. Researchers discovered that an increase in laminate thickness correlates with enhanced resilience to fatigue loading [16].

Plate bending is the deflection of a plate perpendicular to its plane caused by external forces and moments. As a result, it is crucial to analyze how a plate bends [17].

The deformation of circular plates presents a significant challenge within elastic theory. Circular plates are utilized extensively across numerous technological domains. This has captured the interest of many for an extended period. In the design and analysis of structural elements or systems, particularly when it comes to calculating the deflections and bending moments of a thin circular elastic plate subjected to a uniformly distributed load or internal pressure [18].

An appropriate plate theory's differential equation can calculate deflection. Plate stresses may be estimated from these deflections. Failure theories can predict plate failure under a load if stresses are recognized [17].

Using a device specifically designed for this purpose, this paper Research presents an experimental study of the effects of static loads and low-cycle fatigue (LCF) loads on a 0.25 mm thick carbon fiber reinforced polymer sheet until the specimen fails in both tests. The experimental results are compared with the theoretical results based on the maximum deflection of the sheets as a criterion for deformation under internal air pressure as a distributed load and constant boundary conditions.

2. METHODOLOGY FOR EXPERIMENTAL PROCEDURES

It has two sides: the first is the sample used, and the second is the device designed for the experimental procedure.

The specimen used in this experimental study consists of a 3K orthogonal plate CFRP with an epoxy resin matrix. It has a thickness of h = 0.25 mm, with fiber layers oriented at 45°, and dimensions of 350 × 350 mm. The cross-section subjected to the transverse load has a 150 mm circular diameter.

Table 1 shows the mechanical properties of an orthotropic plate of the carbon fiber perpendicular plate after the experimental tensile test, while Table 2 shows the chemical analysis of the sample using the Axia chemiSEM device compared to the results of the American standard Figure 1 illustrates the composition and distribution of elements across the various phases.

Table 1. Mechanical properties of carbon fiber in an orthotropic context

Parameter	Symbol	Value	Unit
Elastic Modulus in X	Ex	$250*10^9$	N/m^2
Elastic Modulus in Y	Ey	$280*10^9$	N/m^2
Elastic Modulus in Z	Ez	$280*10^9$	N/m^2
Shear Modulus in XY	Gxy	$340*10^9$	N/m^2
Shear Modulus in YZ	Gyz	$150*10^9$	N/m^2
Shear Modulus in XZ	Gxz	$370*10^9$	N/m^2
Poisson's Ratio in XY	Vxy	0.38	-
Poisson's Ratio in YZ	Vyz	0.3	-
Poisson's Ratio in XZ	Vxz	0.3	-
Tensile Strength in X	Rmx	$750*10^6$	N/m^2
Tensile Strength in Y	Rmy	$1201*10^6$	N/m^2
Yield Strength in X	Rpx	$690*10^6$	N/m^2
Yield Strength in Y	Rpy	$977*10^6$	N/m^2
Mass Density	ρ	1790	Kg/m^3

Table 2. Analysis of the chemical composition of carbon fiber-reinforced polymer

Type of Test	C%	O %	CI%	NI%	Other
Standard	75	22	0.3	0.1	0.5
Experimental	77.6	21.8	0.4	0.2	0.5

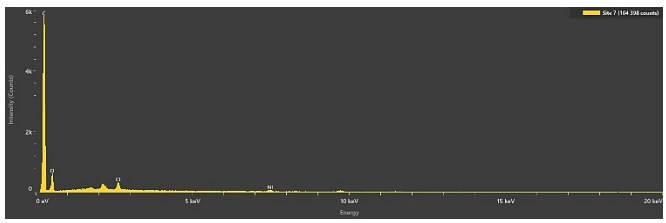

Figure 1. The distribution of CFRP elements

The device was designed based on a system that efficiently regulates internal air pressure from an air compressor, which can generate a maximum pressure of 1 MPa. Pressure control is managed through a manual valve, allowing precise adjustments within a range of 0 to 4 MPa. The regulated pressure is then directed to an inlet solenoid valve, which operates with a closing force varying from 0 to 4 MPa. This

valve facilitates the controlled transfer of compressed air into a cast iron test cylinder, which has a thickness of 5 mm and a transverse diameter of 150 mm.

The cylinder features an open-top transverse space, serving as a window for the uniformly applied pressure at the center of the sample, which is securely fixed to the top of the test cylinder. A pressure sensor with a sensing range of 0 to 4 MPa is mounted on the cylinder wall to ensure accurate pressure measurement within the test cylinder.

A digital displacement disk, positioned on top of the cylinder, monitors load-induced sample deformation. This disk makes contact with the sample surface through a sensor tube, detecting the maximum deviation during deformation within a range of 0 to 26 mm, with an accuracy of 0.01 mm. After the designated pressure retention period, the outlet solenoid valve releases the pressure from the cylinder.

The procedural sequence of the device components is interconnected through carbon steel connecting pipes, which have a thickness of 3.7 mm and a length of 1200 mm, running from the air compressor to the outlet solenoid valve. The entire system is primarily controlled by a PLC-based control unit, which regulates the timing of compressed air entry, the duration of air retention within the cylinder, and its controlled release.

The controller enables the repetition of the procedure under identical conditions across multiple cycles, supporting a cycle range of 0 to 999, with a timing interval between cycles of 0 to 999 seconds and a pressure retention delay of 0 to 999 seconds. The device is capable of performing both static and fatigue tests, including low-cycle fatigue testing, which requires repeated loading cycles. Figures 2 and 3 display the two programming interfaces used for test automation.

The experiment was conducted at room temperature, with loads being gradually and consistently increased in both tests until specimen failure. Figure 4 illustrates the experimental system used in this study, while Figure 5 provides a schematic representation of the apparatus, detailing its components.

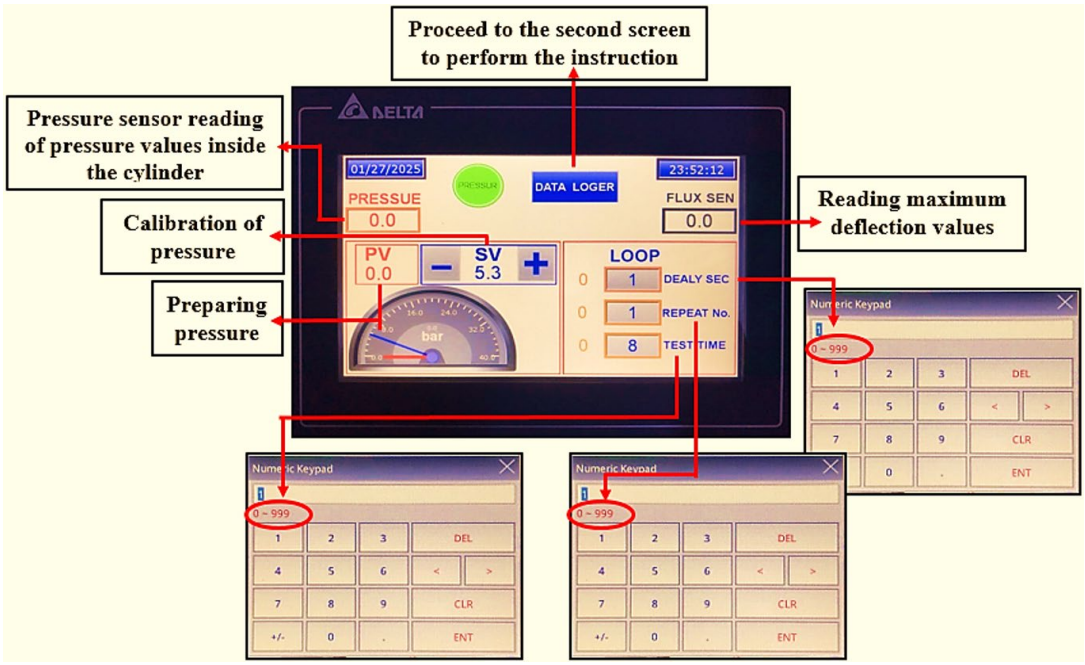

Figure 2. The specifics of the first settings configuration screen

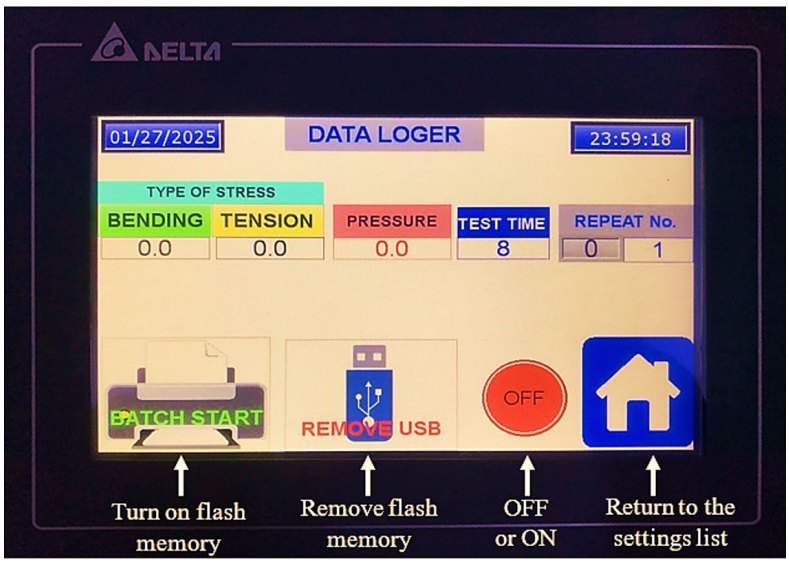

Figure 3. The second screen that applies first-screen settings

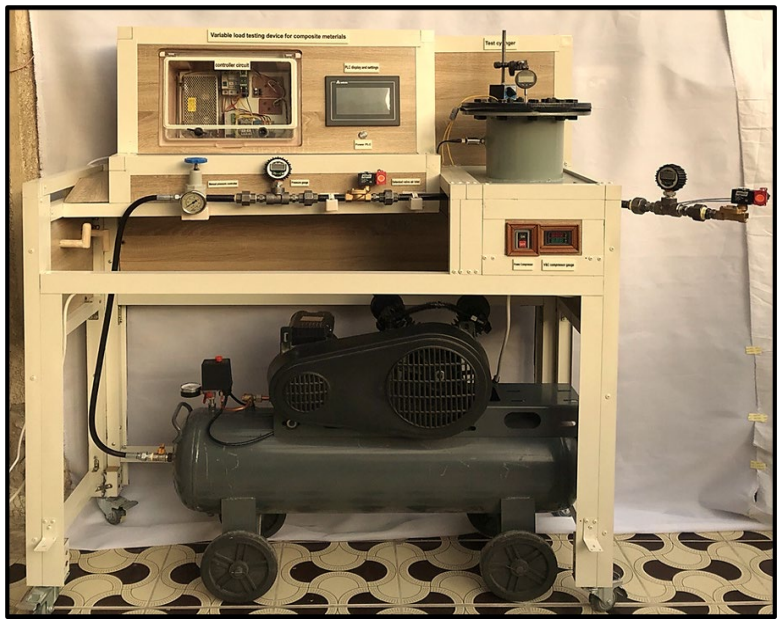

Figure 4. The utilized experimental system

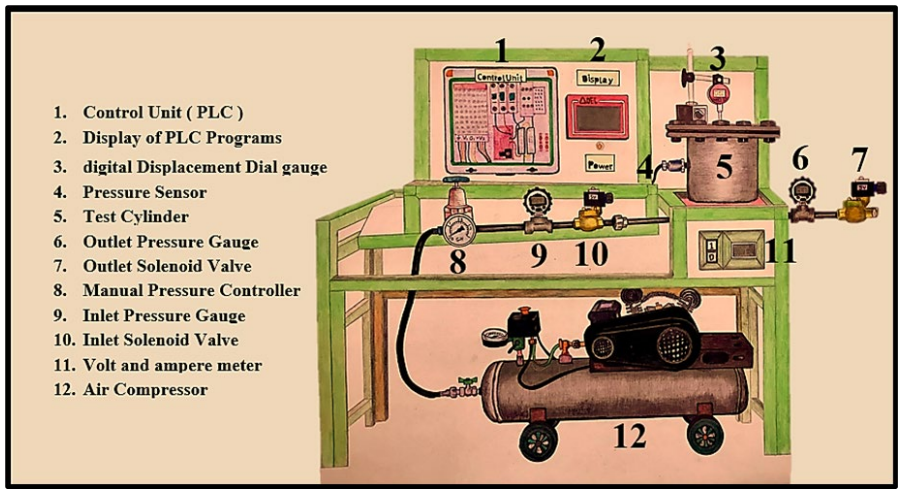

Figure 5. The experimental system's schematic diagram

3. FUNDAMENTAL MATHEMATICAL EQUATIONS FOR UNIFORMLY DISTRIBUTED LOADS

3.1 Analysis of large deflections in orthotropic thin plates

It is assumed that the principal axes of the circle's diameter, which is subjected to the applied load, align parallel with the principal directions of the orthotropic material. When an orthotropic circular plate with radius (a) and a uniform applied load (q) is set up with a = b, it is expressed by Eq. (1) [19].

$$W = \frac{q}{64\,D_1}(a^2 - r^2)^2 \tag{1}$$

where,

$$r = \sqrt{x^2 + y^2} \tag{2}$$

$$D_1 = \frac{1}{8}\left(3D_x + 2H + 3D_y\right) \tag{3}$$

$$H = D_{xy} + 2G_{x_y} \tag{4}$$

$$D_{xy} = \frac{t^3 E'_x v_y}{12\left(1 - v_x v_y\right)} = \frac{t^3 E'_y v_x}{12\left(1 - v_x v_y\right)} \tag{5}$$

$$G_{x_y} = \frac{r^3 \mathrm{G}}{12} \tag{6}$$

$$D_x = \frac{t^3 E'_x}{12\left(1 - v_x v_y\right)} \tag{7}$$

$$D_y = \frac{t^3 E'_y}{12\left(1 - v_x v_y\right)} \tag{8}$$

The stresses that were observed in the center of the composite plate when r = 0, regardless of r and θ, can be articulated as follows:

$$\sigma_r = \sigma_\theta = \frac{3q}{4}\left[\frac{a}{h}\right]^2 \tag{9}$$

The tensile strain at the center of the plate during significant

deflections of the composite material may be determined by study [20].

$$\varepsilon_r = \varepsilon_\theta = 0.462\frac{w^2}{a^2} \tag{10}$$

The tangential strain (ε_t) and effective strain (ε_{eff}) experienced by the composite plate can be determined using the following equations [21]:

$$\varepsilon_t = -[\varepsilon_r + \varepsilon_\theta] \tag{11}$$

$$\epsilon_{e_{ff}} = \sqrt{\frac{2}{3}\left(\varepsilon_r^2 + \varepsilon_\theta^2 + \varepsilon_t^2\right)} \tag{12}$$

3.2 Mechanical considerations of fatigue fracture

An analysis of stress and strains under cyclic loading is essential for engineering applications. In certain practical applications, the material functions under constant maximum and minimum stress levels. This is referred to as constant amplitude stressing. The mean stress, σ_m, is the average of the maximum σ_{max} and minimum σ_{min} stress values, and the algebraic difference is the difference between the maximum and minimum stress values, $\Delta\sigma = \sigma_{max} - \sigma_{min}$. The half range is referred to as stress amplitude. The following are the mathematical expressions [22]:

$$\sigma_m = \frac{\sigma_{max} + \sigma_{min}}{2} \tag{13}$$

$$\sigma_a = \frac{\sigma_{max} - \sigma_{min}}{2} \tag{14}$$

The stress ratio R is defined as the ratio of minimum stress to maximal stress and is:

$$R = \frac{\sigma_{min}}{\sigma_{max}} \tag{15}$$

where, R=1 denotes the static tensile load.

3.3 Experimental findings comparing the two tests and discussion

Two composite carbon fiber samples, each with a uniform thickness of 0.25 mm, were selected for the experimental test. Pressures ranging from 1 bar to the value leading to the complete collapse of both samples were applied to the 150 mm diagonal cross-sectional area. Using a disc displacement gauge set at r = 0, the maximum deflection values of the samples were recorded. The samples were firmly placed on the test cylinder, and the experimental test was initiated using the specially designed testing mechanism.

In both static loading and fatigue testing under constant load, the deformation of the samples resulted in convexity as the applied loads increased. This deformation exhibited linear behavior, with deflection values in the fatigue test under constant load exceeding those recorded in the static loading test. The fatigue test mechanism stabilized maximum deflection values after several cycles of constant loading, explaining this disparity.

In the static loading test, when a load of 6×10^5 N/m² was applied, the deformation increased steadily until a cracking sound was detected, indicating microstructural damage in the sample. As the pressure increased further, reaching 6.2×10^5 N/m², the deformation briefly escalated, leading to instantaneous failure characterized by an explosive rupture of the circular plate's diameter.

Similarly, during the fatigue test under constant load, an audible fracture indication was observed at the same applied load of 6×10^5 N/m², specifically during the crack initiation stage. As the applied load increased to 6.5×10^5 N/m², the internal structural cracking sounds became more pronounced, signaling the transition to the crack propagation stage, where microcracks expanded and became more visible within the material's microstructure. The applied stress was gradually raised to a total load of 6.8×10^5 N/m², at which point the cracking noise intensified significantly, accompanied by a noticeable increase in maximum deflection. After 15 cycles of cyclic loading, the specimen suffered complete and explosive failure, similar to the behavior observed under static loading conditions. However, the fragmentation of the plate was more pronounced, with smaller scattered sections, compared to its state under static loading. This observation suggests a gradual structural failure during cyclic loading, commonly referred to as fatigue failure.

A summary of the key mechanisms influencing CFRP panel performance under different loading conditions (static and fatigue) can be outlined as follows:

•The maximum deflection values under static loading were lower than those recorded in the fatigue test. This is attributed to the single application of force in static loading, whereas the fatigue test involves multiple loading cycles, allowing deflection to accumulate over time.

•The duration for crack propagation and damage manifestation in fatigue testing was longer due to the cyclic nature of loading. The brief intervals between cycles allowed damage to accumulate gradually, unlike static loading, where failure occurred more abruptly.

•The appearance of the failed CFRP sample varied between the two loading conditions. After fatigue failure, the sample exhibited a more fragmented and crumbled state compared to its failure under static loading.

Figure 6 illustrates the sample during testing, while Figure 7 presents the two samples after failure. Image (a) depicts the sample post-failure under static loading, whereas Image (b) shows the sample after failure under fatigue loading. Table 3 compares the maximum deflection values for both tests, and Figure 8 provides a graphical comparison of the maximum deflection values.

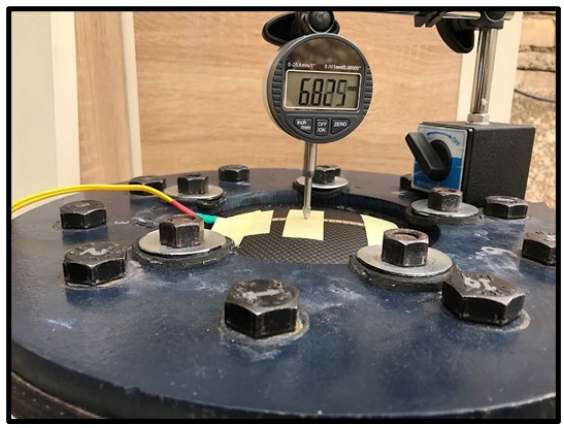

Figure 6. CFRP specimen under 5×10^5 N/m² distributed compression test

Table 3. Experimental aberration results for static load and fatigue under constant load conditions

Under Static Load		Fatigue Under Constant Load	
Pressure × 10^5 N/m²	**Experimental Max. Deflection mm**	**After a Number of Cycles**	**Experimental Max. Deflection mm**
1	2.30	27	2.56
2	3.65	33	3.72
3	4.84	33	5.06
4	5.94	29	6.16
5	7.23	25	7.36
6.2	8.975 failure	31	9.24
6.5		11	9.72
6.8	-	15	12.32 failure

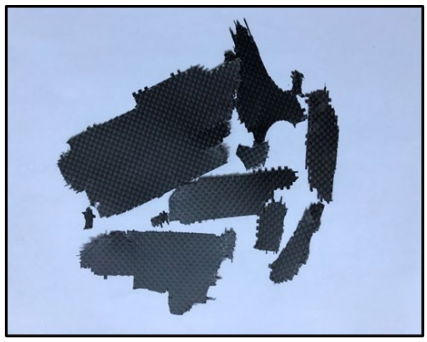

(a) The specimen under static loading

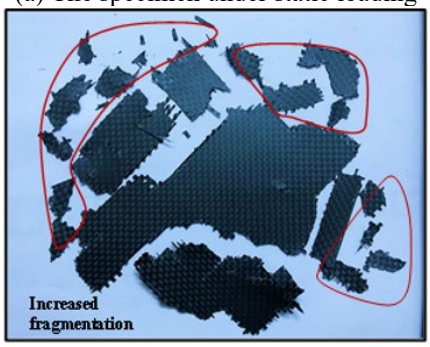

(b) The specimen under cyclic loading

Figure 7. The scattered section of the sample was subjected to static loading compared to that under cyclic loading

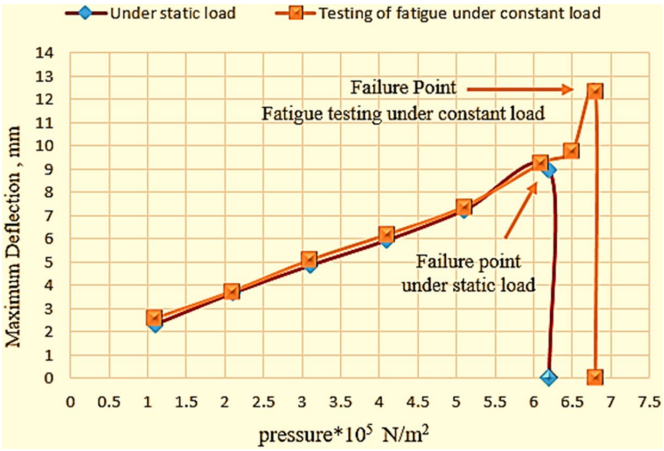

Figure 8. The maximum deflection resulting from static load and fatigue under constant load

3.4 SEM microstructure analysis and Vickers hardness testing

The microstructure of the CFRP sample was examined microscopically after exposure to low-cycle stresses. Figure 9 presents the microscopic analysis of the sample before failure, while Figure 10 depicts the sample after failure, consisting of two images:

•Image (a) illustrates the initial deterioration of the matrix and the formation of microcracks. This phase involves the development and expansion of fractures in regions with a high concentration of voids, as the applied loads increase.

•Image (b) shows the critical stress concentration at the fracture tips, reaching its peak at 6.8 × 10^5 N/m², ultimately leading to the specimen's failure.

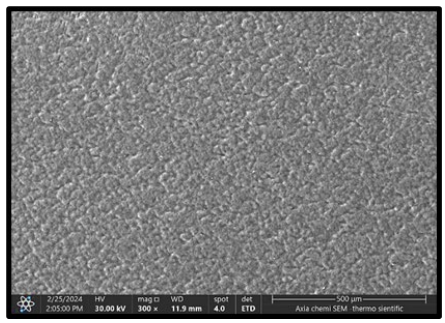

Figure 9. SEM image for CFRP specimen before testing

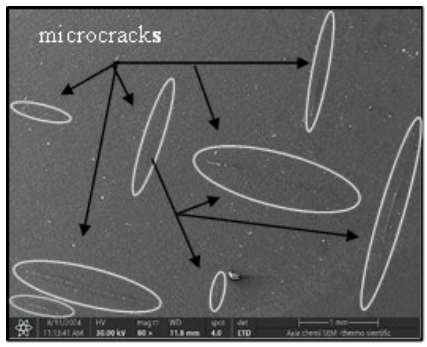

(a) Matrix damage following testing

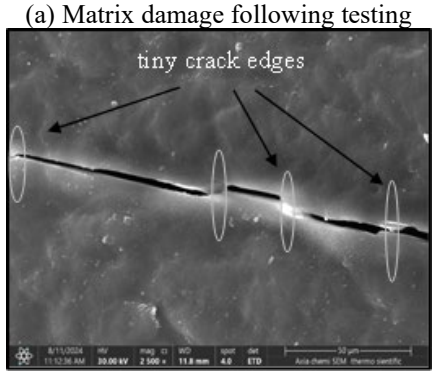

(b) Stress-induced fractures on tiny crack edges

Figure 10. Images of the microstructure of a CFRP sample subsequent to fatigue testing under constant load

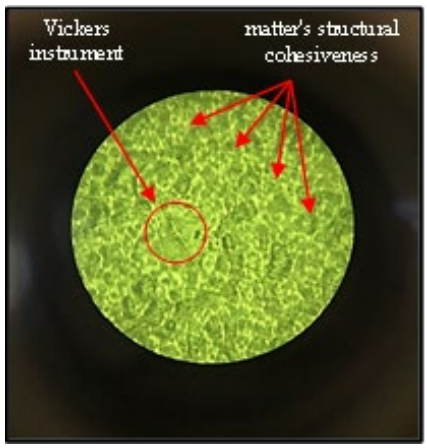

(a) Before the experimental

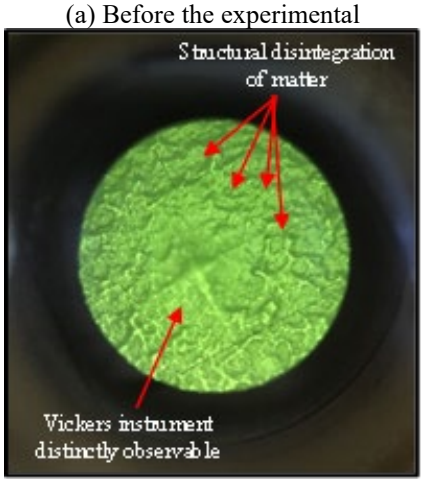

(b) After the experimental

Figure 11. Microscopic views of the CFRP specimen utilized for Vickers hardness testing

A Vickers hardness test was conducted on the specimen before the experimental procedure, using an applied load of 500 g for 15 seconds, with three readings taken from different locations on the sample. The test yielded an average hardness of 111.33 H.V. Figure 11 (a) illustrates the hardness test conducted before the experimental procedure.

Following the experimental test, another Vickers hardness test was performed under the same conditions to assess the hardness of the failed specimen. The hardness measurement after failure was 28.22 H.V., as shown in Figure 11 (b). This significant reduction in hardness indicates material degradation and a deterioration of the internal structure due to the applied loads.

Figure 11 provides a microscopic image demonstrating the impact of the Vickers hardness test tool on the sample:

•Image (a) represents the sample condition prior to testing.

•Image (b) displays the sample condition after failure, highlighting the structural changes caused by the applied stresses.

Scanning electron microscope analysis is essential for identifying the stages of structural failure in specimens subjected to different stresses and loads; the material hardness test before and after the experimental procedure is also considered one of the most important evidence for determining these stages.

3.5 Theoretical vs. Experimental outcomes

The experimental results of the sample deformation stages were compared with the theoretical results, focusing on the maximum deflection under an ascending load gradient. This study utilized Tables 4, 5, and 6 to calculate the maximum deflection, stresses, and strains experienced by the sample due to both theoretically and experimentally applied loads. Figures 12, 13, and 14 present graphical representations of the results derived from these tables.

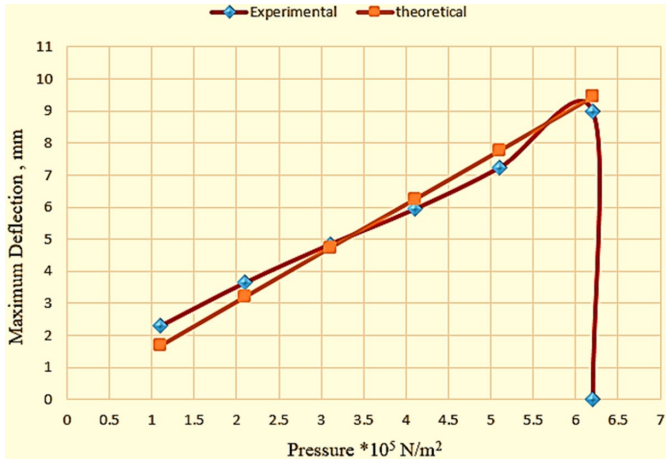

Figure 12. Experimental deflection under static load vs theoretical deflection of CFRP material

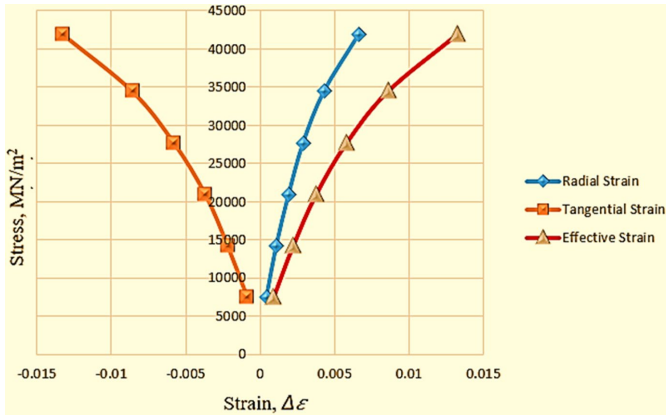

Figure 13. Relationship between strain and stress based on experimental results of maximum deflection of CFRP

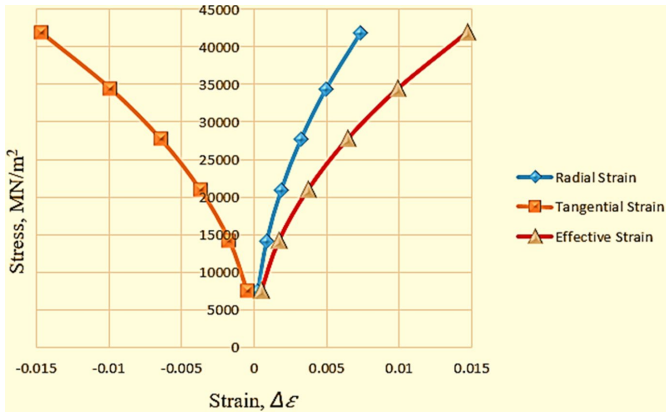

Figure 14. The relationship between the applied load and strain based on the theoretical findings of CFRP

The experimental findings identified four key phases in relation to the theoretical maximum deflection outcomes:

Initial Phase:

A distributed load of 1 × 10^5 N/m² caused the sample to adopt a convex shape.

The difference between the theoretical and experimental deflection values can be attributed to the application of significant deviation theory, which does not fully capture the slight variations observed in the experimental data.

Second and Third Phases:

The theoretical and experimental values closely aligned, with only minor discrepancies observed.

These phases demonstrated a strong correlation between predicted and actual deflections.

Fourth Phase:

At 6.2 × 10^5 N/m², the difference between the theoretical and experimental deflection values became more pronounced.

The experimental data recorded the complete collapse of the sample, whereas the theoretical model continued to provide readings with consistent differences.

This discrepancy arises because the theoretical model does not account for sudden failure, whereas the experimental results reflect the actual structural breakdown of the sample.

Considering the inherent uncertainty in material properties due to industrial defects, the experimental results demonstrated strong convergence with theoretical predictions. This alignment allows for reliable scientific conclusions, as highlighted in the comparison table provided below.

Table 4. Deflections of CFRP material: Experimental vs. theoretical under static load

Pressure × 10^5 N/m²	Experimental Deflection / mm	Theoretical Deflection / mm
1	2.30	1.68
2	3.65	3.21
3	4.84	4.74
4	5.94	6.25
5	7.23	7.77
6.2	8.975 failure	9.45

Table 5. Maximum stresses and strains for CFRP center experimental deflection

Pressure × 10^5 N/m²	Stress MN/m²	Radial Strain $\varepsilon r = \varepsilon\theta$	Tangential Strain (εt)	Effective Strain (εeff)
1	7425	0.0004345	-0.0008690	0.000869
2	14175	0.0010942	-0.0021884	0.0021884
3	20925	0.001924	-0.003691	0.0037439
4	27675	0.002898	-0.005796	0.0057959
5	34425	0.0042933	-0.008587	0.0085867
6.2	41850	0.0066159	-0.013232	0.0132318

Table 6. Maximum stresses and strains for CFRP center theoretical deflection

Pressure × 10^5 N/m²	Stress MN/m²	Radial Strain $\varepsilon r = \varepsilon\theta$	Tangential Strain (εt)	Effective Strain (εeff)
1	7425	0.000231813	-0.0004636	0.0004636
2	14175	0.000846310	-0.0016926	0.0016926
3	20925	0.001845334	-0.0036907	0.0036907
4	27675	0.003208333	-0.0064167	0.0064167
5	34425	0.004958628	-0.0099173	0.0099173
6.2	41850	0.007334712	-0.0146694	0.0146694

Table 5 presents the relationship between stress and strain based on the maximum experimental deflection, as illustrated in Figure 13. This relationship remains linear from the initial loading phase until it begins to deviate from linearity during the early stages of laminate matrix damage, occurring under a load of 4 × 10^5 N/m². The deflection continues to increase until the damage reaches its peak, culminating in structural failure at the maximum load, where the maximum deflection values correspond to the stresses that lead to the complete collapse of the specimen.

Table 6 presents the theoretical strain values corresponding to stresses at the maximum theoretical deflection, with Figure 14 illustrating their trajectory. The agreement between the experimental and theoretical results demonstrates a high level of convergence, with a strain progression pattern in response to the applied loads that closely matches the experimental data.

In fatigue testing under constant load, the maximum deflection values require a longer duration to reach stabilization. The deflection measurements reflect the sample deformation caused by the cyclic loading technique, in which each load is applied in repeated cycles. This approach extends the stabilization period of deflections and results in higher deflection values compared to static loading conditions.

All variations observed in the first cycle correspond to those recorded under static loading, where each pressure value is applied in a single batch. The theoretical predictions regarding maximum deflection closely align with the experimental findings.

Figure 15 illustrates the relationship between the number of cycles and the maximum deflection values for each applied load. The black marker at the end of each deflection line represents the stability stage of the maximum deflection value, which is reached after several cycles, based on both the experimental test results and the detailed theoretical calculations.

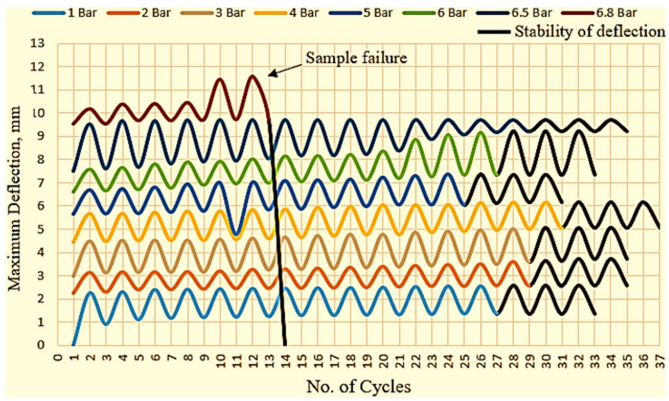

Figure 15. The relationship between the number of cycles and the maximum deflection values during fatigue testing under constant load for CFRP

Table 7 presents the values of maximum stress (σmax), minimum stress (σmin), and mean stress (σm), along with the algebraic difference ($\Delta\sigma$), stress amplitude ($\sigma\alpha$), and stress ratio (R) for loads ranging from 1 to 6.8 × 10^5 N/m². The stress ratio values exhibited an upward trend, aligning with the gradual increase in applied loads until the sample reached failure.

Figure 16 illustrates the relationship between the number of cycles and the stress values corresponding to each applied load. The graphs indicate that:

•As the loads increase, the stress values also increase.

•Higher loads result in higher stress values.

•The ratios between increasing stress values gradually decrease until they converge at peak loads.

This trend suggests a reduction in panel stiffness, attributed to the deterioration of the microstructure and the propagation of cracks throughout the sample. Ultimately, the sample fails under an applied load of 6.8×10^5 N/m² during cycle 14.

Table 7. Results of testing fatigue under constant load for all applied load levels for CFRP specimen

Pressure × 10^5 N/m²	σ_{max} / MN/m²	σ_{min} / MN/m²	σ_m / MN/m²	σ_α / MN/m²	Δ_σ / MN/m²	R
1	7425	2025	4725	2700	5400	0.27
2	14175	7425	10800	3375	6750	0.52
3	20925	14175	17550	3375	6750	0.68
4	27675	20925	24300	3375	6750	0.76
5	34425	27675	31050	3375	6750	0.80
6	41175	34425	37800	3375	6750	0.84
6.5	43875	41175	42525	1350	2700	0.94
6.8	45900	43875	44887.5	1012.5	2025	0.96

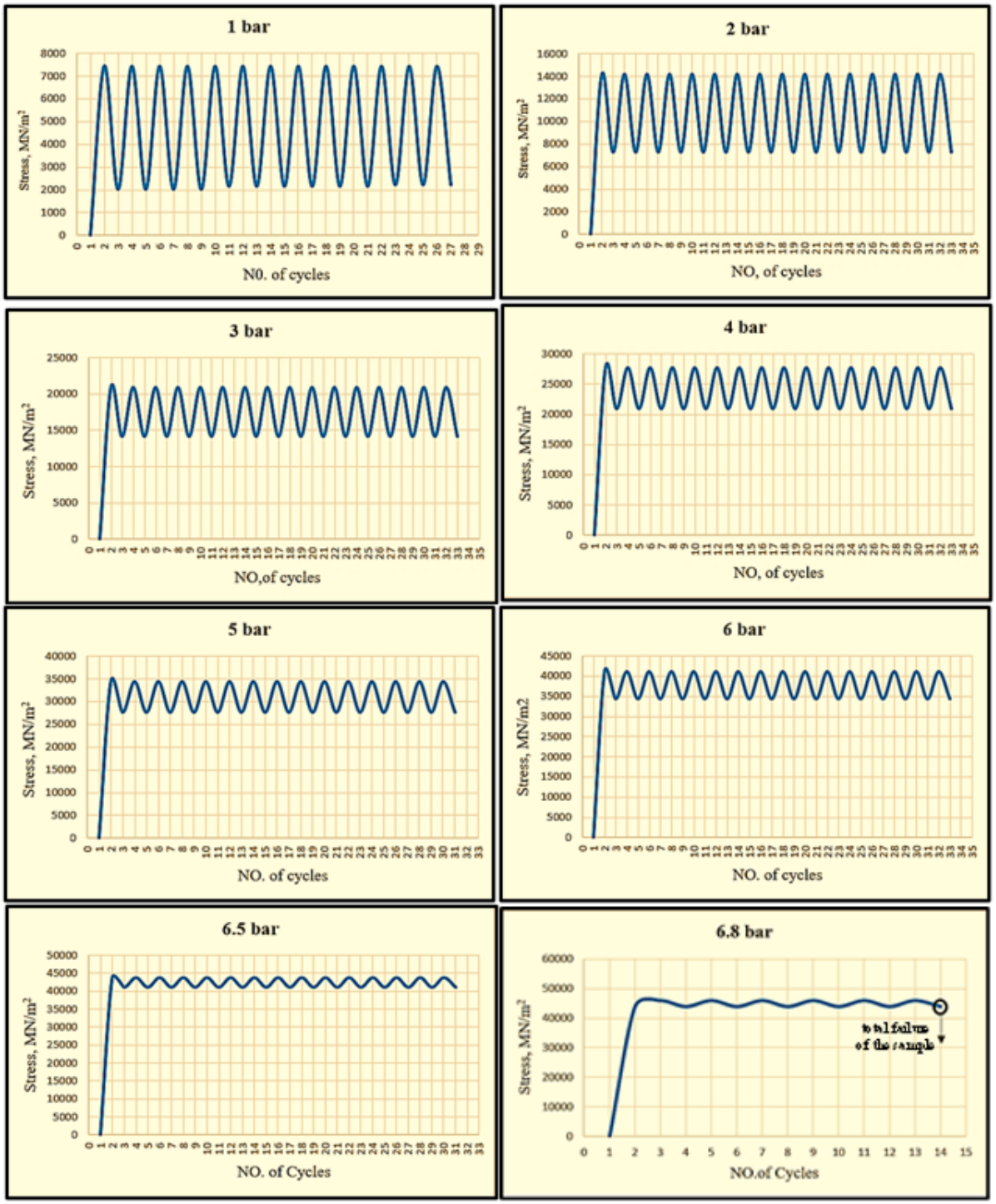

Figure 16. The relationship between the stress values and the number of cycles for each load applied to the CFRP sample

Figure 17 illustrates the relationship between the number of cycles and the resulting strains due to the stresses the plate reached due to the loads applied to the sample. The steadily increasing strain is evident at the maximum applied load of 6.8 × 10^5 N/m^2 due to the high stress the sample was exposed to, which caused its hardness to decline to the point of total collapse.

Figure 18 illustrates the relationship between the number of cycles and the maximum stress attained by the sample, as the maximum deflection stabilizes at the conclusion of the cycles for each applied load. The upper section of the diagram indicates the phase of fiber breakage and total failure of the sample.

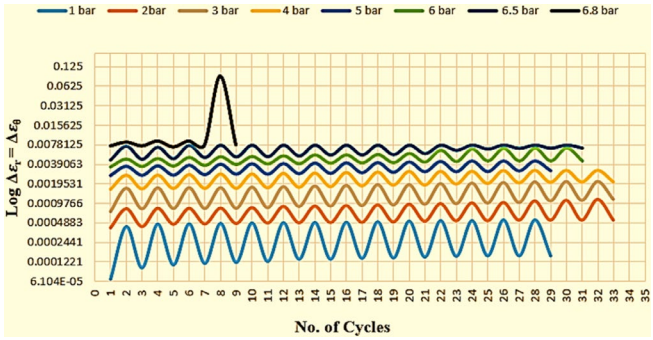

Figure 17. The relationship between strains and the number of cycles in the testing fatigue under a constant load of CFRP

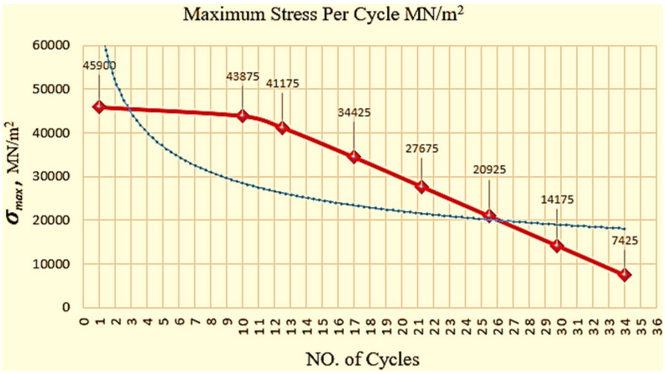

Figure 18. The relationship between the number of cycles at each applied load and the peak stress at the conclusion of each cycle in testing fatigue under a constant load of CFRP

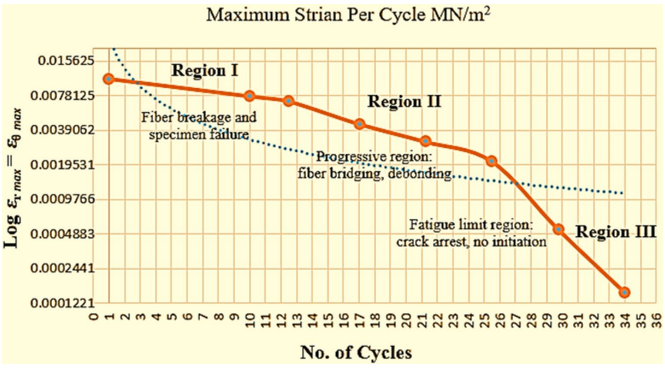

Figure 19. The maximum strain curve at the conclusion of each load cycle ε-N

Fatigue life cannot be determined through more precise regions, as indicated by Figure 19. Consequently, Gamstedt and Talreja [23] proposed the ε-N curve as a method for plotting the strain instead of the stress. This approach enables the identification of more precise regions that correspond to the phases of damage development in three regions. The first region is the fiber fracture region, which occurs at a stress that significantly exceeds the material's yield stress. The second region is the average stress, which is the region that marks the onset of cracking and its gradual proliferation. The third region is the non-failure region, which is the region that immediately precedes the matrix's fatigue limit region.

4. CONCLUSION

The device used in the experimental test was built on solid foundations and high-precision software control of the sequence of operations and wide time ranges through which composite materials can be tested under different pressures and loads, whether they are regularly or unevenly graded and under static or dynamic loads in a practical and somewhat accurate manner.

The phases of sample deformation exhibited comparable linear behavior in both experiments, regardless of whether the sample was subjected to static loading or fatigue testing under constant load. However, at elevated pressures, distinct variations were observed in the values of maximum deviations and strains induced by the resultant radial and circumferential stresses.

Under static loading, the internal structure of the sample fractured at 6 × 10^5 N/m², leading to total collapse at the peak load of 6.2 × 10^5 N/m², with a maximum deflection of 8.975 mm.

In fatigue testing under constant load, at a load of 6 × 10^5 N/m², fracture initiation occurred at a location distant from the signs of total failure. Damage persisted through multiple cycles, progressing through three distinct stages: Crack initiation, microcrack growth, significant crack growth, also referred to as crack propagation.

The pressure gradient continued to increase until it reached its maximum at 6.8 × 10^5 N/m², at which point the sample completely failed, with a maximum deflection of 12.32 mm.

The failure mode analysis was further validated through microscopic examination conducted after testing. The experimental results demonstrated strong convergence with the theoretical predictions, reinforcing the study's findings.

The key observations from the two tests can be summarized as follows:

•The specimen experienced a complete collapse during the static test, which occurred shortly after the internal structure began to deteriorate. The maximum deflection recorded was 8.975 mm.

•The internal structure of the specimen began to show signs of deterioration early during the low-cycle fatigue test, ultimately collapsing after a longer duration and a deflection of 12.32 mm, indicating a gradual degradation at lower stress levels compared to the static test.

•The material's elevated hardness resulted in the specimen's explosive failure in both tests, as the stored potential energy was released as a single impulse at the highest load peak following significant degradation of hardness.

•The hardness of the CFRP sheet recorded a significant deterioration on the Vickers scale after the sample was subjected to complete failure due to applied pressures, reaching 28.22 H.V compared to its hardness before the experimental procedure, which was 111.33 H.V.

•The static test makes it difficult to foresee the specimen's complete failure, while the fatigue test allows for incremental material deterioration that may be monitored and built upon before the specimen collapses.

Recommendations for future practical implementations

•Employing an additional composite material in conjunction with CFRP during the tests, maintaining identical thickness, and assessing the performance of both materials in terms of fatigue resistance.

•Employing an isotropic material in conjunction with CFRP of identical thickness to evaluate the fatigue resistance performance of orthotropic materials relative to isotropic materials.

•Performing low-cycle fatigue testing with fluctuating loads. This facilitates the observation of damage and its progression in accordance with practical applications that align more closely with real-world scenarios.

•Conducting tests within a high-temperature range (above room temperature) as high temperatures influence materials' fatigue resistance and susceptibility to damage.

REFERENCES

[1] Kaw, A.K. (2005). Mechanics of Composite Materials. CRC Press.

[2] Harris, B. (1999). Engineering Composite Materials. The Institute of Materials, London

[3] Sánchez-Gálvez, V., Gálvez, F., Sancho, R., Cendón, D. (2017). A new analytical model to simulate high-speed impact onto composite materials targets. International Journal of Impact Engineering, 108: 322-333. https://doi.org/10.1016/j.ijimpeng.2017.04.024

[4] Ishida, H., Kumar, G. (2013) Molecular characterization Of Composite Interfaces. Springer.

[5] Katunin, A. (2015). Stone impact damage identification in composite plates using modal data and quincunx wavelet analysis. Archives of Civil and Mechanical Engineering, 15(1): 251-261. https://doi.org/10.1016/j.acme.2014.01.010

[6] Hashin, Z. (1981). Fatigue failure criteria for unidirectional fiber composites. Journal of Applied Mechanics, 48(4): 846-852. https://doi.org/10.1115/1.3157744

[7] Bobba, S., Leman, Z., Zainudin, E.S., Sapuan, S.M. (2020). Low Velocity Impact and Internal Pressure Behaviors of Unaged E-Glass and S-Glass/Epoxy Composite Elbow Pipe Joints. Journal of Pipeline Systems Engineering and Practice, 11(4): 04020043. https://doi.org/10.1061/(ASCE)PS.1949-1204.0000493

[8] Abdel-Magid, B., Lopez-Anido, R., Smith, G., Trofka, S. (2003). Flexure creep properties of E-glass reinforced polymers. Composite Structures, 62(3-4): 247-253. https://doi.org/10.1016/j.compstruct.2003.09.022

[9] Uusitalo, K. (2013). Designing in carbon fibre composites. Master thesis, Chalmers University of Technology.

[10] Lind, A. (2013). Utmattning av järnvägsbroar i armerad betong. https://www.diva-portal.org/smash/get/diva2:654837/FULLTEXT01.pdf.

[11] Guo, R., Li, C., Niu, Y., Xian, G. (2022). The fatigue performances of carbon fiber reinforced polymer composites–a review. Journal of Materials Research and Technology, 21: 4773-4789. https://doi.org/10.1016/j.jmrt.2022.11.053

[12] Vassilopoulos, A.P., Keller, T. (2011). Fatigue of Fiber-Reinforced Composites. Springer Science & Business Media.

[13] Weber, I., Schwartz, P. (2001). Monitoring bending fatigue in carbon-fibre/epoxy composite strands: A comparison between mechanical and resistance techniques. Composites Science and Technology, 61(6): 849-853. https://doi.org/10.1016/S0266-3538(01)00028-8

[14] Couillard, R.A.A., Schwartz, P. (1997). Bending fatigue of carbon-fiber-reinforced epoxy composite strands. Composites science and technology, 57(2): 229-235. https://doi.org/10.1016/S0266-3538(96)00134-0

[15] Naderi, M., Maligno, A.R. (2012). Fatigue life prediction of carbon/epoxy laminates by stochastic numerical simulation. Composite Structures, 94(3): 1052-1059. https://doi.org/10.1016/j.compstruct.2011.11.013

[16] Tai, N.H., Ma, C.C.M., Lin, J.M., Wu, G.Y. (1999). Effects of thickness on the fatigue-behavior of quasi-isotropic carbon/epoxy composites before and after low energy impacts. Composites Science and Technology, 59(11): 1753-1762. https://doi.org/10.1016/S0266-3538(99)00037-8

[17] Mojahedin, A., Jabbari, M., Khorshidvand, A.R., & Eslami, M.R. (2016). Buckling analysis of functionally graded circular plates made of saturated porous materials based on higher order shear deformation theory. Thin-Walled Structures, 99: 83-90. https://doi.org/10.1016/j.tws.2015.11.008

[18] Wang, Y., Xu, R., Ding, H. (2010). Three-dimensional solution of axisymmetric bending of functionally graded circular plates. Composite Structures, 92(7): 1683-1693. https://doi.org/10.1016/j.compstruct.2009.12.002

[19] Ugural, A.C. (2009). Stresses in Beams, Plates, and Shells. CRC Press.

[20] Timoshenko, S. (1959). Theory of Plates and Shells. McGraw-Hill.

[21] Hosford, W.F., Caddell, R.M. (2011). Metal Forming: Mechanics and Metallurgy. Cambridge University Press.

[22] Khalifeh, A. (2023). Perspective Chapter: Fatigue of Materials. In Failure Analysis-Structural Health Monitoring of Structure and Infrastructure Components. IntechOpen. https://doi.org/10.5772/intechopen.107400

[23] Gamstedt, E.K., Talreja, R. (1999). Fatigue damage mechanisms in unidirectional carbon-fibre-reinforced plastics. Journal of Materials Science, 34: 2535-2546. https://doi.org/10.1023/A:1004684228765

NOMENCLATURE

CFRP	Fiber-Reinforced Polymer composites
LCF	Low-Cycle fatigue
SEM	Scanning electron microscope
3K	3000 individual strands combined
C	Carbon
O	Oxygen
CI	Chlorin
Ni	Nickel
W	Maximum deflection
a	Radius of plate
b	Outer radius of plate
h	Thickness of plate

D	Flexural rigidity
q	Intensity of distributed load per unit N/m^2
σ_r	Normal components of the membrane stresses in N/m^2
σ_θ	Cylindrical coordinates
ε_r	Radial
ε_θ	Polar strains
ε_t	Tangential strain
$\epsilon_{e_{ff}}$	Effective strain
σ_m	Mean stress
σ_a	Stress amplitude N/m^2
$\Delta\sigma$	Algebraic difference N/m^2